Stability and Robustness Analysis and Improvements for Incremental Nonlinear Dynamic Inversion Control

van 't Veld, Ronald; van Kampen, Erik-Jan; Chu, Qiping

DOI
10.2514/6.2018-1127

Publication date
2018

Document Version
Accepted author manuscript

Published in
Proceedings of the 2018 AIAA Guidance, Navigation, and Control Conference

Stability and Robustness Analysis and Improvements for Incremental Nonlinear Dynamic Inversion Control

R. C. van 't Veld, E. van Kampen and Q. P. Chu

Delft University of Technology, Delft, Zuid-Holland, 2629 HS, the Netherlands

Incremental nonlinear dynamic inversion (INDI) is a variation on nonlinear dynamic inversion (NDI), retaining the high-performance characteristics, while reducing model dependency and increasing robustness. After a successful flight test with a multirotor micro aerial vehicle, the question arises whether this technique can be used to successfully design a flight control system for aircraft in general. This requires additional research on aircraft characteristics that could cause issues related to the stability and performance of the INDI controller. Typical characteristics are additional time delays due to data buses and measurement systems, slower actuator and sensor dynamics, and a lower control frequency. The main contributions of this article are 1) an analytical stability analysis showing that implementing discrete-time INDI with a sampling time smaller than 0.02s results in large stability margins regarding system characteristics and controller gains; 2) a simulation study showing significant performance degradation requiring controller adaptation due to actuator measurement bias, angular rate measurement noise, angular rate measurement delay and actuator measurement delay; and 3) the use of a real-time time delay identification algorithm based on latency to successfully synchronize the angular rate and actuator measurement delay together with pseudo control hedging (PCH) to prevent oscillatory behavior.

Nomenclature

A_x, A_y, A_z	Specific forces along body X/Y/Z axis, m/s^2
b, $\bar{c}$	Wing Span and Mean aerodynamic chord, m
C_l, C_m, C_n	Dimensionless Rolling, Pitching and Yawing moment coefficients
F, G	Linearized System and Control effectiveness matrix
g	Gravity constant, m/s^2
I	Inertia matrix, kg·m^2
K	Gain
k, N	Variable number
$\underline{M}$	Aerodynamic moment vector, Nm
m	Mass, kg
n_y	Normalized specific force along body Y axis, g
p, q, r	Roll, Pitch and Yaw rates around the body X/Y/Z axis, rad/s
$\hat{R}$	Average square difference function estimator
S	Wing area, m^2
s	Laplace variable
T, t	Sampling time and Time, s
u	Physical control input
u, v, w	Velocity components along body X/Y/Z axis, m/s
V	Velocity, m/s
x	State
z	Complex variable for z-transform
β, ϕ, θ	Sideslip, Roll and Pitch angle, rad
γ	Control effectiveness uncertainty ratio
δ	Control surface deflection, rad

ζ	Filter damping ratio
μ	Bias mean
ν	Virtual control input
ρ	Air density, kg/m^3
σ	Noise variance
τ	Variable number
Φ, Γ	Discrete System and Control effectiveness matrix
$\underline{\omega}$	Angular rate vector, rad
ω_n	Filter natural frequency, rad/s
Subscript	
a, e, r	Aileron, Elevator and Rudder
c, d, u, x	Commanded, Desired, Actuator, Control
h, rm	Hedge, Reference model
k	Discrete index
0	Current point in time

I. Introduction

Before the 1990s, the design of almost all flight control laws for aircraft was based on classical control techniques.[1,2] However, in recent years the use of advanced, multivariable control techniques has become the standard. Moreover, nonlinear dynamic inversion (NDI) has been the most popular technique of these advanced, multivariable techniques. The advantage of NDI over classical techniques is that NDI avoids gain-scheduling, directly incorporates nonlinearities into the control laws and isolates the handling quality dependent part of the control laws from the airframe/engine dependent part.[3,4]

These advantages ultimately result in improved performance and reduced development cost and time. Furthermore, NDI can be used to improve safety by avoiding aircraft accidents due to loss of control in flight.[5] This is important as two surveys from 1993 to 2007 and from 2006 to 2011 show that loss of control has consistently been an important cause of fatal accidents as well as fatalities.[6,7] Within the 2006 to 2011 period, loss of control in flight even was the most import cause of fatalities.

A drawback of NDI is that model mismatches and measurement errors reduce performance and can even result in unstable situations.[8] In light of these issues, the development of incremental nonlinear dynamic inversion (INDI) was triggered. INDI is a variation on NDI retaining the advantages of NDI, while decreasing the controller dependency on the vehicle model. As result, the controller robustness regarding model uncertainties and measurement errors is increased.[8] Moreover, these benefits are obtained by relatively simple means compared to, for example, the extension of NDI with neural networks.[9] Therefore, using INDI to design the flight control system (FCS) of an aircraft can also be beneficial regarding controller certification.[10]

INDI shows promising results compared with NDI in simulation studies applied to various aeronautical and space vehicles.[8,11,12] However, in practice INDI has only been flight tested twice. The first test was performed within the VAAC Harrier aircraft, but the test was merely a proof of concept at a time when INDI had not been thoroughly investigated yet.[13] Recently, INDI was successfully applied to a multirotor micro aerial vehicle (MAV) confirming the results obtained in simulations.[14]

Due to the successful application of INDI in a multirotor MAV, the question arises whether using INDI to design FCSs could contribute to safer, cheaper aircraft with shorter development periods, straightforward certification and increased performance. However, before a flight test is performed, additional research on aircraft characteristics that could cause issues related to the stability and performance of the INDI controller is required. Typical characteristics are additional time delays due to data buses and measurement systems, slower actuator and sensor dynamics, and a lower controller frequency.[8,12,14] To investigate these characteristics, this paper applies INDI to a model of the PH-LAB Cessna Citation, a CS-25 certified fixed-wing aircraft, co-owned by Delft University of Technology.

This paper presents three main contributions. First, the closed-loop system stability of a general linear system controlled by INDI is investigated as a sampled-data system, i.e. a system with a continuous-time plant and a discrete-time controller. As such, the effect of time delay, control gain, control effectiveness uncertainty and controller frequency on INDI stability is investigated. Second, the effect of real-world phenomena, e.g. sensor bias, noise and time delays, on an INDI controlled aircraft are investigated. Third,

the paper provides solutions to prevent performance degradation of the INDI controlled system due to any of the investigated real-world phenomena significantly affecting controller performance.

The outline of the paper is as follows. Sec. II shows the derivation of discrete-time INDI compared to continuous-time INDI. Sec. III discusses the investigation of the stability of discrete-time INDI. Sec. IV describes the development of two attitude controllers, based on INDI and PID control. The effect of real-world phenomena on these controllers is investigated in Sec. V. Moreover, Sec. V also provides solutions to prevent performance degradation due to these phenomena based on literature. Additionally, Sec. VI presents a real-time time delay identification method essential to compensate for unsynchronized time delay. Finally, Sec. VII gives the conclusions and recommendations.

II. Incremental Nonlinear Dynamic Inversion

Originally, INDI was developed for continuous-time systems. However, INDI has to be developed as discrete-time controller to be able to investigate the closed-loop system as sampled-data system. The derivation of continuous-time INDI is reviewed to support the derivation of discrete-time INDI.

A. Continuous-time INDI

The continuous-time INDI derivation starts from a general nonlinear system, see Eq. (1).[8,12]

$$\dot{\underline{x}} = \underline{f}(\underline{x}, \underline{u}) \tag{1}$$

The system of Eq. (1) can be linearized about the current point in time indicated by the subscript '0', see Eq. (2). As such, the variables $\underline{x}_0$, $\dot{\underline{x}}_0$ and $\underline{u}_0$ are given by the latest available measurements, while the variables $\underline{x}$, $\dot{\underline{x}}$ and $\underline{u}$ are in the future. Note that the linearization is based on the assumptions of a small sampling time and instantaneous control effectors.

$$\begin{aligned}
\dot{\underline{x}} &\approx \underline{f}(\underline{x}_0, \underline{u}_0) + \left.\frac{\partial \underline{f}(\underline{x}, \underline{u})}{\partial \underline{x}}\right|_{\underline{x}=\underline{x}_0, \underline{u}=\underline{u}_0} (\underline{x} - \underline{x}_0) + \left.\frac{\partial \underline{f}(\underline{x}, \underline{u})}{\partial \underline{u}}\right|_{\underline{x}=\underline{x}_0, \underline{u}=\underline{u}_0} (\underline{u} - \underline{u}_0) \\
\dot{\underline{x}} &\approx \dot{\underline{x}}_0 + F(\underline{x}_0, \underline{u}_0)(\underline{x} - \underline{x}_0) + G(\underline{x}_0, \underline{u}_0)(\underline{u} - \underline{u}_0)
\end{aligned} \tag{2}$$

The time-scale separation principle is assumed to hold for Eq. (2). The change in control input, $\underline{u}$, is considered significantly faster than the change in system state, $\underline{x}$, based on the assumptions of small sampling time and instantaneous control effectors.[12] Thus, assuming $\underline{x} \approx \underline{x}_0$ while $\underline{u} \neq \underline{u}_0$. As a result $\underline{x} - \underline{x}_0 = 0$ is assumed, which can be used to simplify Eq. (2) to Eq. (3). Eq. (3) can be used to develop a control law by defining the virtual control input as $\underline{\nu} = \dot{\underline{x}}$. Concluding, the physical control input u can be computed using Eq. (4), the latest available measurements ($\dot{\underline{x}}_0$,$\underline{x}_0$,$\underline{u}_0$) and the virtual control input, $\underline{\nu}$. This virtual control input is to be designed. Moreover, the control effectiveness matrix, $G(\underline{x}_0, \underline{u}_0)$ of the system has to be known and invertible.

$$\dot{\underline{x}} = \dot{\underline{x}}_0 + G(\underline{x}_0, \underline{u}_0)(\underline{u} - \underline{u}_0) \tag{3}$$

$$\underline{u} = \underline{u}_0 + G^{-1}(\underline{x}_0, \underline{u}_0)(\underline{\nu} - \dot{\underline{x}}_0) \tag{4}$$

B. Discrete-time INDI

The start of the derivation of discrete-time INDI is equal to the continuous-time INDI derivation, including all assumptions, up to Eq. (3). Eq. (3) can be seen as the combination of two linear state-space systems, Eqs. (5) and (6), both with $F(\underline{x}_0, \underline{u}_0) = 0$.

$$\dot{\underline{x}} = F(\underline{x}_0, \underline{u}_0)\underline{x} + G(\underline{x}_0, \underline{u}_0)\underline{u} \tag{5}$$

$$\dot{\underline{x}}_0 = F(\underline{x}_0, \underline{u}_0)\underline{x}_0 + G(\underline{x}_0, \underline{u}_0)\underline{u}_0 \tag{6}$$

The discrete counterpart of such a linear state-space systems is known, Eq. (7).[15] Considering that $F(\underline{x}_0, \underline{u}_0) = 0$, Eq. (7) can be simplified to Eq. (8).

$$\begin{gathered}
\underline{x}_{k+1} = \Phi(\underline{x}_0, \underline{u}_0)\underline{x}_k + \Gamma(\underline{x}_0, \underline{u}_0)\underline{u}_k \\
\Phi = I + \Delta t F + \frac{\Delta t^2}{2!}F^2 + \frac{\Delta t^3}{3!}F^3 + \cdots \qquad \Gamma = \Delta t G + \frac{\Delta t^2}{2!}FG + \frac{\Delta t^3}{3!}F^2G + \cdots
\end{gathered} \tag{7}$$

$$\frac{\underline{x}_{k+1} - \underline{x}_k}{\Delta t} = G(\underline{x}_0, \underline{u}_0)\underline{u}_k \tag{8}$$

Using Eq. (8) to discretize both Eqs. (5) and (6) and combining these as in Eq. (3) results in Eq. (9). Eq. (9) is rewritten by defining $\underline{x}_{0_k} = \underline{x}_{k-1}$ and $\underline{u}_{0_k} = \underline{u}_{k-1}$ to obtain Eq. (10), based on the definition of the '0' subscript in continuous-time. These definitions imply that the variables with the 'k-1' subscript are given by the latest available measurements.

$$\frac{\underline{x}_{k+1} - \underline{x}_k}{\Delta t} = \frac{\underline{x}_{0_{k+1}} - \underline{x}_{0_k}}{\Delta t} + G(\underline{x}_{0_k}, \underline{u}_{0_k})(\underline{u}_k - \underline{u}_{0_k}) \tag{9}$$

$$\frac{\underline{x}_{k+1} - \underline{x}_k}{\Delta t} = \frac{\underline{x}_k - \underline{x}_{k-1}}{\Delta t} + G(\underline{x}_{k-1}, \underline{u}_{k-1})(\underline{u}_k - \underline{u}_{k-1}) \tag{10}$$

Eq. (10) can be inverted to obtain the discrete-time INDI control law, Eq. (11). However, the direct inversion of Eq. (10) would require the future state $\underline{x}_k$ to be known. To obtain a usable control law, the term $\frac{\underline{x}_k - \underline{x}_{k-1}}{\Delta t}$ is considered to represent the forward difference approximation of $\dot{\underline{x}}_{k-1}$ and can be replaced by the backward difference approximation $\frac{\underline{x}_{k-1} - \underline{x}_{k-2}}{\Delta t}$.

$$\underline{u}_k = \underline{u}_{k-1} + G^{-1}(\underline{x}_{k-1}, \underline{u}_{k-1}) \left(\underline{\nu}_k - \frac{\underline{x}_{k-1} - \underline{x}_{k-2}}{\Delta t} \right) \tag{11}$$

$$\underline{\nu}_k = \frac{\underline{x}_{k+1} - \underline{x}_k}{\Delta t} \tag{12}$$

Concluding the physical control input u_k can be computed using Eq. (11), the latest available measurements ($\underline{x}_{k-1}$,$\underline{u}_{k-1}$), the previous measurements, $\underline{x}_{k-2}$, and the virtual control input, $\underline{\nu}_k$. This discrete-time virtual control input is again to be designed, similar to continuous-time INDI. Moreover, the control effectiveness matrix, $G(\underline{x}_{k-1}, \underline{u}_{k-1})$ of the system has to be known and invertible.

III. Analytical Stability

The stability of the theoretically developed INDI control law of Eq. (11) is analyzed for a general mathematical system with actuator dynamics, see Fig. 1. To keep the analysis clear, only a single-input single-output first-order linear system is used, Eq. (13), together with a first-order actuator, Eq. (14). Moreover, the virtual control input is designed based on a simple P-controller with gain K_x, Eq. (15). First, the effect of the mathematical system characteristics in combination with the controller sampling time are analyzed for the baseline system. Afterwards, the effect of variations based on time delay and control effectiveness uncertainty on the closed-loop stability are presented.

$$\dot{x} = Fx + Gu \tag{13}$$

$$\dot{u} = K_u(u_c - u) \tag{14}$$

$$\nu_k = K_x(x_{d_k} - x_{k-1}) \tag{15}$$

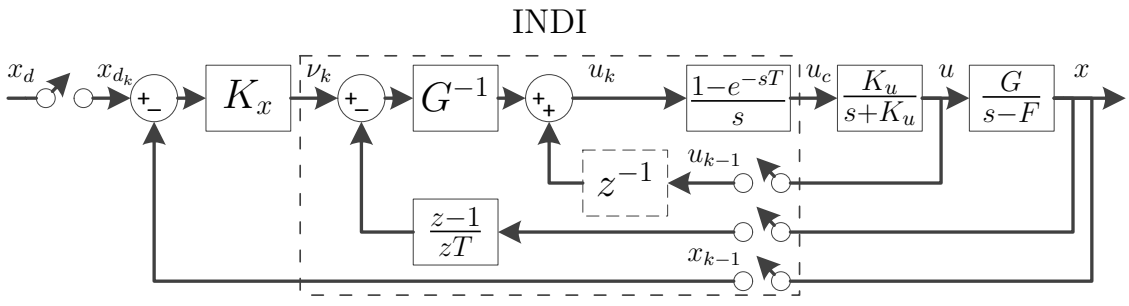

Figure 1: Sampled-data system with discrete-time INDI controller and continuous-time linear system

A. Analysis Method

The closed-loop system of Fig. 1 contains both continuous- and discrete-time components as well as samplers and a zero-order hold block, $\frac{1-e^{-sT}}{s}$, converting continuous signals into discrete signals and vice verse. The discrete equivalent of the sampled-data system has to be found to analyze the system. This discrete equivalent is found by adding phantom samplers and rearranging the block diagram, such that there are samplers in front and behind all continuous (series of) transfer function(s). The combination of the two samplers with the continuous (series of) transfer function(s) can then be converted to a discrete transfer function via tables combining z- and s-transforms.[16]

The discrete-time system can be reduced to a single transfer function. The characteristic polynomial of this transfer function can then be used for the stability analysis. Note that the system is asymptotically stable if and only if all roots of the characteristic polynomial have a magnitude smaller than one. To avoid having to solve all the roots of the characteristic polynomial, Jury's stability criterion is used to check the system's stability based on a tabular method.[17]

B. Baseline System

First, the stability of a baseline system without time delays or control effectiveness uncertainties is investigated. The baseline closed-loop system used is the system depicted in Fig. 1 with the dashed unit delay block not included. The stable regions of the baseline INDI controller are given in Fig. 2. The constant values, $F = 2$, $K_u = 13$ and $K_x = 7$, used throughout the figures were selected to obtain stability regions typical for the PH-LAB Cessna Citation model. Note that the closed-loop stability is independent of the control effectiveness matrix when uncertainties are not considered.

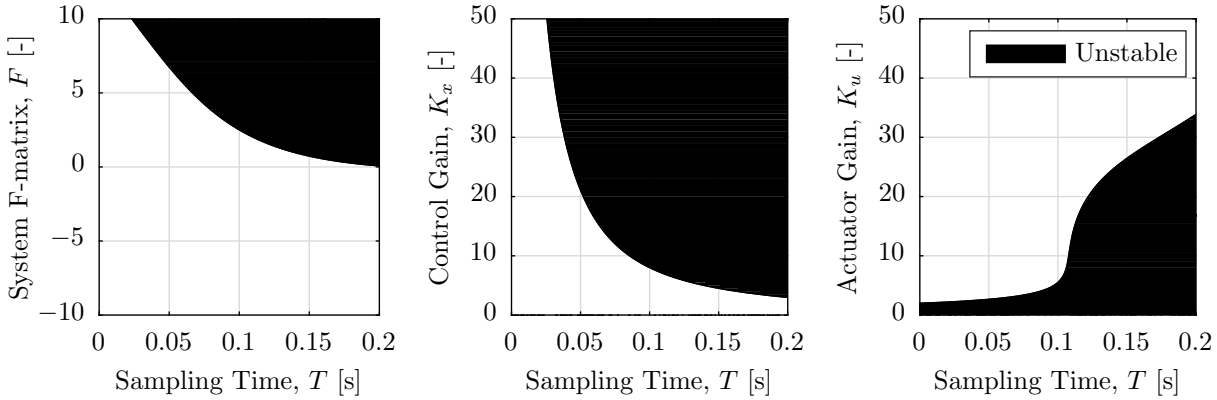

(a) $K_u = 13$, $K_x = 7$ (b) $F = 2$, $K_u = 13$ (c) $F = 2$, $K_x = 7$

Figure 2: Stability for baseline INDI controller

In general, logical trends can be observed regarding the stability of the baseline INDI controller. Fig. 2a shows that systems implemented with smaller sampling time can control systems with less natural stability, i.e. a higher F-matrix value. Similarly, Figs. 2b and 2c show that the same conclusion can be drawn for more aggressive control laws, i.e. a higher control gain, and slower actuators, i.e. a lower actuator gain.

Another observation based on Fig. 2 is that the system is stable for sampling times smaller than 0.02s in all three figures. The only exception is a system with small actuator gains, however this instability is not a result of any discrete effects as the same unstable region appears when analyzing a continuous-time controller. Unfortunately, nonlinear effects like control saturation and system nonlinearities are not included within the analysis. Moreover, the effect of multiple inputs, multiple outputs, multirate feedback signals and multiloop controllers can be added to the analysis to increase the accuracy of the results. Therefore, it is difficult to set a maximum sampling time, which would ensure system stability when using a discrete-time INDI controller. Still, a sampling time smaller than 0.02s seems to provide a large stable region regarding variation in F, K_u and K_x when considering the typical values of the PH-LAB Cessna Citation.

C. Measurement Time Delay

The stability of INDI controllers subjected to measurement time delay is an issue for INDI controllers.[8,14] Especially, when the actuator measurements, u_{k-1} and the state derivative measurement, the $\frac{z-1}{zT}$ block, are not equally delayed. Moreover, there is a disagreement whether or not the unit delay of the actuator measurement, u_{k-1}, indicated by the dashed unit delay block in Fig. 1, has to be included[12,14] or not.[11,18] Therefore, four different systems are investigated: 1) a baseline system, Fig. 2c; 2) a system with a unit delay on the state derivative measurement Fig. 3a; 3) a system with a unit delay on the actuator measurement, Fig. 3b; and 4) a system with a unit delay on both actuator and state derivative measurements, Fig. 3c.

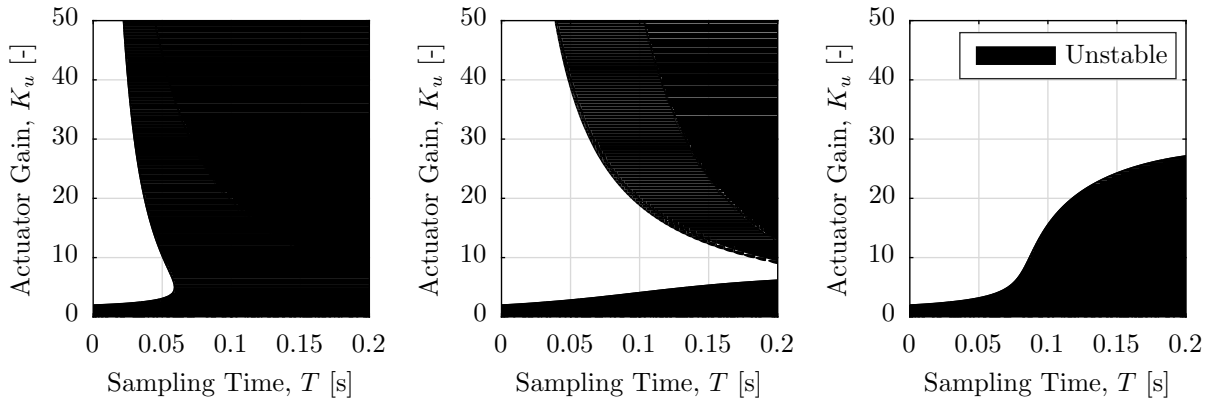

(a) State derivative (b) Actuator (c) Actuator and state derivative

Figure 3: Stability with unit delays on actuator measurements and/or state derivative: $F = 2$, $K_x = 7$

Clearly, the baseline system and the system with both the actuator and state derivative measurements delayed have the largest stable region compared with the systems with either the actuator or state derivative measurements delayed. This shows the importance of delaying both measurement signals equally. Moreover, it shows that when the combination of discrete-time controller and continuous-time system is used, the unit delay of the actuator measurements degrades system stability and should not be included in the controller.

Furthermore, comparing Figs. 2c and 3c shows that the INDI controller can handle some overall time delay within the system. Additionally, there is a significant difference between the tolerance to state derivative delay and actuator delay in Figs. 3a and 3b. This difference is attributed to the fact that the state derivative signal is used via negative feedback, while the actuator measurements are used via positive feedback. Delaying a negative feedback signal results in magnified control inputs, resulting in relatively fast system instability. On the other hand, delaying a positive feedback signal results in damped control inputs, resulting in relatively slow system instability. This effect is also seen in the results of Sec. VI.

D. Control Effectiveness Uncertainties

The stability of INDI controllers subjected to model uncertainties should not be an issue for INDI controllers.[8,14] The results of this section are independent of uncertainties in the system matrix, however control effectiveness uncertainties can still affect the controller. The effect of control effectiveness uncertainties is seen in Fig. 4. The uncertainties have been implemented into the system of Fig. 1 by substituting $(G + \Delta G)^{-1}$ for G^{-1}, the uncertainty ratio used is defined by Eq. (16).

$$\gamma = \frac{G}{G + \Delta G} \tag{16}$$

Fig. 4 shows that the INDI controller remains stable over a large range of control effectiveness uncertainty, given that the controller runs at a sampling time smaller than the aforementioned 0.02s. This conclusion is supported by similar observations made in literature.[12,14] Furthermore, note that the system instability for low and negative values of γ is not the result of any discrete effects and also appears when analyzing a continuous-time closed-loop system.

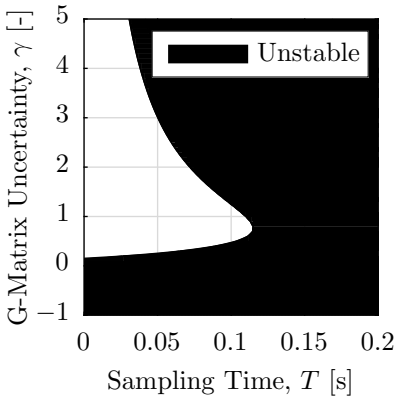

Figure 4: Stability with control effectiveness uncertainty: $F = 2$, $K_u = 13$, $K_x = 7$

IV. Attitude Controller

Two attitude controllers are developed to investigate the effect of real-world phenomena on an INDI controlled aircraft. One controller is based on discrete-time INDI and the other controller is based on PID control. The PID controller is used to put the results obtained with the INDI controller into perspective, see Sec. V. The INDI attitude controller is based on a cascaded design with an angular rate inner loop and attitude outer loop.

A. Angular Rate Inner Loop

The angular rate inner loop is based on Euler's equations of motion, Eq. (17), which is similar in form to Eq. (1). To obtain the discrete-time control law of Eq. (11), the G-matrix is obtained based on Eq. (17), see Eq. (18).[8] Therefore, the angular rate controller is given by Eqs. (19) and (20). Note that the developed inner loop neglects the actuator dynamics of the system and assumes instantaneous control effectors.

$$\dot{\underline{\omega}} = I^{-1}\underline{M} - I^{-1}(\underline{\omega} \times I\underline{\omega}) \tag{17}$$

$$G(\underline{x}_{k-1}, \underline{u}_{k-1}) = I^{-1}\frac{1}{2}\rho V^2 S \begin{bmatrix} bC_{l_{\delta_a}} & 0 & bC_{l_{\delta_r}} \\ 0 & \bar{c}C_{m_{\delta_e}} & 0 \\ bC_{n_{\delta_a}} & 0 & bC_{n_{\delta_r}} \end{bmatrix} \tag{18}$$

$$\underline{u}_k = \underline{u}_{k-1} + \frac{2I}{\rho V^2 S}\begin{bmatrix} bC_{l_{\delta_a}} & 0 & bC_{l_{\delta_r}} \\ 0 & \bar{c}C_{m_{\delta_e}} & 0 \\ bC_{n_{\delta_a}} & 0 & bC_{n_{\delta_r}} \end{bmatrix}^{-1}\left(\underline{\nu}_k - \frac{\underline{\omega}_{k-1} - \underline{\omega}_{k-2}}{\Delta t}\right) \tag{19}$$

$$\underline{\nu} = \begin{bmatrix} \nu_p \\ \nu_q \\ \nu_r \end{bmatrix}; \quad \underline{\omega} = \begin{bmatrix} p \\ q \\ r \end{bmatrix}; \quad \underline{u} = \begin{bmatrix} \delta_a \\ \delta_e \\ \delta_r \end{bmatrix} \tag{20}$$

Similar to Eq. (15) in Sec. III, the virtual control input is designed based on the tracking error. However, the angular rate inner loop uses PI-control instead of just P-control, because the integral controller can compensate for potential bias in the actuator measurements, as further explained in Sec. V. The overall control structure and tuning is presented in Sec. IV.D.

B. Attitude Outer Loop

The attitude outer loop consist of the control of the roll, pitch and sideslip angles. The sideslip angle is preferred above the yaw angle, as a controller aimed at keeping the sideslip angle at zero results in coordinated flight. The principle of time-scale separation is used to develop the roll and pitch angle outer loop around

the angular rate inner loop. The slow outer loop is defined such that the output is used as input of the faster inner-loop. As such, the dynamics of the inner-loop are neglected and the angular rates are assumed to be equal to the commanded values. The relation between attitude angles and angular rates is based on a kinematic equation independent of aircraft characteristics, see Eq. (21). Therefore, this loop is based on the standard NDI technique instead of INDI.

$$\begin{bmatrix} \dot{\phi} \\ \dot{\theta} \end{bmatrix} = \begin{bmatrix} 1 & \sin\phi\tan\theta & \cos\phi \\ 0 & \cos\phi & -\sin\phi\tan\theta \end{bmatrix} \begin{bmatrix} p \\ q \\ r \end{bmatrix} \tag{21}$$

To obtain the NDI outer loop Eq. (21) is inverted. Moreover, the attitude rates, $\dot{\phi}$ and $\dot{\theta}$, are replaced by the virtual control inputs ν_ϕ and ν_θ respectively. Similar to INDI these virtual control inputs are designed based on tracking error, but for this loop only P-control is used. The r_c is based on the separate sideslip outer loop designed next and as discussed before, the p_c and q_c are used as inputs for the inner loop. The roll and pitch outer loop is given by Eq. (22).

$$\begin{bmatrix} p_c \\ q_c \end{bmatrix} = \begin{bmatrix} 1 & \sin\phi\tan\theta \\ 0 & \cos\phi \end{bmatrix}^{-1} \left\{ \begin{bmatrix} \nu_\phi \\ \nu_\theta \end{bmatrix} - \begin{bmatrix} \cos\phi\tan\theta \\ -\sin\phi \end{bmatrix} r_c \right\} \tag{22}$$

The control law used for the sideslip outer-loop is given by Eq. (23), which is equivalent to the control law used by Miller.[19] Mathematically, the sideslip outer loop can be developed similar to the roll and pitch outer loop.[20] However, the PH-LAB Cessna Citation does not have accurate, fast sensors measuring the required body velocities (u, v, w) and sideslip angle itself. Therefore, the sideslip controller cannot be based on Eq. (24) and several assumptions are made such that Eq. (23) is obtained. The coordinated flight is the main purpose of the sideslip outer-loop, therefore the sideslip angle, β, and its derivative, $\dot{\beta}$, are assumed zero and consequently $v = 0$. Moreover, it is assumed that the effect of the wp term is negligible. The overall control structure and tuning is presented in Sec. IV.D.

$$r_d = \frac{g}{V}(n_y + \sin\phi\cos\theta) \tag{23}$$

$$\dot{\beta} = \frac{1}{\sqrt{u^2+w^2}} \left(\frac{-uv}{V^2}(A_x - g\sin\theta) + \left(1 - \frac{v}{V^2}\right)(A_y + g\sin\phi\cos\theta) - \frac{vw}{V^2}(A_z + g\cos\phi\cos\theta) + wp - ur \right) \tag{24}$$

C. Pseudo Control Hedging

An important concern for NDI and INDI based controllers is the violation of the assumptions made regarding instantaneous actuator and inner loop dynamics.[12,21] These dynamics are not actually instantaneous and actuators also have position and rate limits introducing control saturation into the closed-loop system. Unfortunately, no solutions were found in literature that completely eliminate the performance degradation that can arise from breaking these assumptions.

Pseudo control hedging (PCH) is used by several authors to at least alleviate the performance degradation issues due to control saturation.[12,21] PCH reduces the magnitude of the commanded signals to a level achievable by the saturated controller.[22] PCH has two potential benefits for the controller developed in this paper. First, PCH can act as an anti-windup technique for the PI-controller used to compute the virtual control input of the inner loop.[21] Second, as explained next PCH adds an additional tunable variable to the system, which can be used to tune the influence of various feedback signals on controller performance, see Sec. VI. Therefore, PCH is selected to complement the developed angular rate inner loop.

PCH consist of a first-order reference model (RM), which imposes the desired dynamics on the output, Eqs. (25) and (26). Moreover, the RM can provide the derivative of the command signal, $\underline{\nu}_{rm}$ which is used as feedforward control term. The RM is adjusted to an achievable level by the command hedge $\underline{\nu}_h$, Eq. (27). However, since $\underline{u}_k$ is not known the command hedge is computed for the previous time step, see Eq. (28). Note that the command hedge can also be computed internally using the desired control input in combination with an actuator model, instead of measuring $\underline{u}_{k-1}$.[21]

$$\underline{\nu}_{rm} = K_{rm}(\underline{\omega}_c - \underline{\omega}_{rm}) \tag{25}$$

$$\underline{\omega}_{rm} = \frac{1}{s}(\underline{\nu}_{rm} - \underline{\nu}_h) \tag{26}$$

$$\underline{\nu}_h = \underline{\nu}_c - \underline{\nu}$$

$$\underline{\nu}_h = \left[\frac{\underline{x}_{k-1} - \underline{x}_{k-2}}{\Delta t} + G(\underline{x}_{k-1}, \underline{u}_{k-1})(\underline{u}_{c_k} - \underline{u}_{k-1})\right] - \left[\frac{\underline{x}_{k-1} - \underline{x}_{k-2}}{\Delta t} + G(\underline{x}_{k-1}, \underline{u}_{k-1})(\underline{u}_k - \underline{u}_{k-1})\right] \tag{27}$$

$$\underline{\nu}_h = G(\underline{x}_{k-1}, \underline{u}_{k-1})(\underline{u}_{c_k} - \underline{u}_k)$$

$$\underline{\nu}_h = I^{-1}\frac{1}{2}\rho V^2 S \begin{bmatrix} bC_{l_{\delta_a}} & 0 & bC_{l_{\delta_r}} \\ 0 & \bar{c}C_{m_{\delta_e}} & 0 \\ bC_{n_{\delta_a}} & 0 & bC_{n_{\delta_r}} \end{bmatrix} (\underline{u}_{c_{k-1}} - \underline{u}_{k-1}) \tag{28}$$

Due to the use of the RM, each INDI loop has an additional tunable variable. The K_{rm} imposes the general desired dynamics on the system, while the linear controller used within the original INDI loop can be used to further adapt some fine dynamics and characteristics of the system. The overall controller structure combining the angular rate inner loop with PCH and the attitude outer loop is presented in Fig. 5. As discussed, the linear controllers (LCs) used to design the virtual control inputs are based on PID-control.

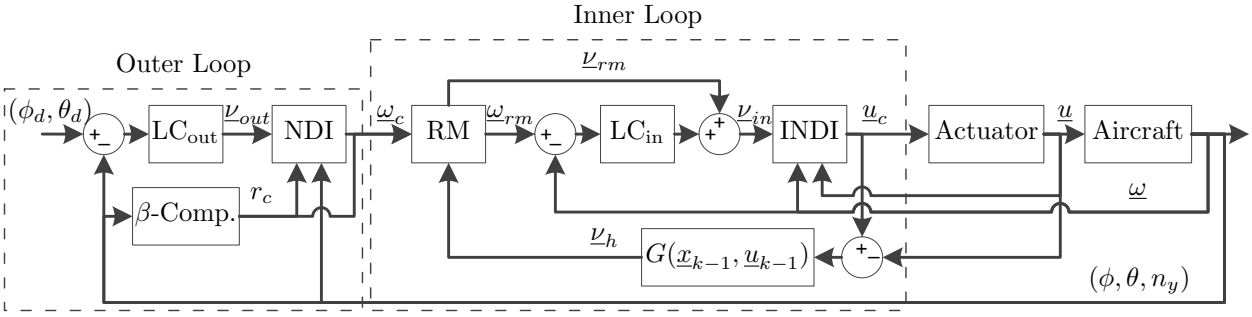

Figure 5: Attitude controller structure based on NDI, INDI and PCH

D. Controller Tuning and PID Controller

The control gains used to tune the developed controller depicted in Fig. 5 are lised in Table 1. Note that initially, the inner loop LC was based on PI-control, while the inner loop RM used P-control. However, as discussed in Sec. V this solution did not perform as expected and a solution using an inner loop based on P-control for the LC and PI-control for the RM was adopted. Furthermore, the controller without PCH used in Sec. VI uses the RM gains as LC gains as this controller does not have a RM.

Table 1: PID and INDI control gains

Channel	PID				INDI			
	Inner		Outer		Inner			Outer
	K_P	K_I	K_P	K_D	$K_{P_{in}}$	$K_{P_{rm}}$	$K_{I_{rm}}$	$K_{P_{out}}$
Roll, p-ϕ	-0.4	-0.75	1.5	0	20	7	1.4	1.5
Pitch, q-θ	-0.4	-1.0	1.5	0	20	6	1.2	1.5
Yaw, r-n_y	-0.4	-0.75	-1.0	-0.3	20	7	1.4	n.a.

A controller based on PID control is developed, besides the INDI controller, to support the investigation on the effect of real-world phenomena on the INDI controller, see Sec. V. The inner loop of the PID controller controls the angular rates (p, q, r), just like the INDI controller. The outer loop of the PID controller controls the attitude angles (ϕ, θ) together with the lateral acceleration (n_y). The lateral acceleration is used to minimize the sideslip angle. Similar to INDI, the sideslip angle itself cannot be used as the PH-LAB Cessna Citation does not have accurate, fast sensors measuring the sideslip angle or body velocities. The PID controller combines an PI-control inner loop with a PD-control outer loop, see Table 1.

V. Effect of Real-World Phenomena on INDI Controlled Aircraft

Before a flight test with an INDI controlled aircraft is performed in future research as follow up on the flight test with INDI in a multirotor MAV, the effect of real-world phenomena on an INDI controlled aircraft are investigated. For this investigation, the controller developed in the previous section is implemented together with the PH-LAB Cessna Citation model.

A. Real-World Phenomena to be Investigated

The two previous flight tests with INDI provide an indication which real-world phenomena are most important to investigate. However, as only two flight tests have been performed, also flight tests with NDI controllers are used within this section.

First, bias, defined as all constant disturbances, is considered. Bias can be introduced into the system as input to the airframe, e.g. wind, and as addition to measured feedback signals. Both NDI and INDI have shown to reject bias as input to the airframe during flight tests.[14,20] However, other flight test have shown that NDI performance can degrade due to severe winds and erroneous measurements.[23,24] Therefore, bias is included as phenomenon that should be investigated.

Second, the topic of discretization is considered. The effect of controller frequency is included in the investigation to confirm the theoretical findings of Sec. III. Other discretization effects can be found in feedback signals through sampling and quantization. The effect of feedback signal sampling times is investigated to complement the investigation on controller frequency. Feedback signal quantization is mentioned as an issue in two flight tests with NDI, however both studies had relatively limited computation resources compared to today's standards.[24,25] Therefore, quantization is not expected to become in issue in any future flight test and quantization will not be investigated.

Third, the effect of model mismatches is considered. The outstanding robustness of INDI with respect to model mismatches was already shown on an MAV.[14] Additionally, almost every simulation study available on the topic of INDI has shown the robustness of INDI. As such, the inclusion of model mismatches is deemed superfluous. Especially, since Sec. III also showed that INDI remains stable over a large range of control effectiveness uncertainty.

Fourth, noise, defined as all random disturbances, will be included in the simulation. Analogous to bias, noise appears as input to the airframe as well as in feedback signals. Flight test have shown that NDI performance can degrade due to severe turbulence and erroneous measurements.[23,24] Moreover, noise within feedback systems is reported for both NDI and INDI to potentially degrade controller performance.[13,20]

Fifth, it is also important to include time delays, as already indicated in Sec. III. This is also confirmed in literature as time delay, for example, caused system instability through a pilot induced oscillation.[4]

The magnitude of all real-world phenomena used in this section is based on previous flight test data with the PH-LAB Cessna Citation, see Table 2. The bias acting on the feedback signals is based on the mean of the disturbances, while the noise acting on the signals is based on the variances of the disturbances. Moreover, a constant wind is implemented as bias with a total velocity of 25 m/s split across all three axes. Additionally, atmospheric turbulence is implemented as noise using the Dryden model with $\sigma = 1\text{m}^2/\text{s}^2$ and $L_g = 150\text{m}$.[15]

Table 2: PH-LAB Cessna Citation real-world phenomena characteristics

	Bias [μ]	Noise [σ^2]	Delay [s]	Sampling Time [s]
p, q, r [rad/s]	$3 \cdot 10^{-5}$	$4 \cdot 10^{-7}$	0.128	0.0192
V [m/s]	2.5	$8.5 \cdot 10^{-4}$	0.1	0.0625
δ_a, δ_e, δ_r [rad]	$4.5 \cdot 10^{-3}$	$5.5 \cdot 10^{-7}$	0.0397	0.01
ϕ, θ [rad]	$4 \cdot 10^{-3}$	$1 \cdot 10^{-9}$	0.128	0.0192
n_y [g]	$2.5 \cdot 10^{-3}$	$1.5 \cdot 10^{-5}$	0.128	0.0192

B. Results

The effect of the real-world phenomena on the controller performance is investigated using 40 second simulation runs. Each run includes four consecutive 3211 maneuvers on the roll and pitch angles starting at an altitude of 6000 m and a velocity of 100 m/s. Both PID and INDI controllers run at 100 Hz, while the PH-LAB model is simulated using variable sampling time to emulate continuous-time. Previous flight test with the PH-LAB aircraft also ran experimental controllers at 100 Hz and according to the results of Sec. III this should result in a stable closed-loop system.

The controller performance is assessed using the sum of the root mean square (RMS) tracking errors of the outer loop control variables (ϕ, θ, β). Tables 3 and 4 show the RMS tracking error for the PID and INDI controllers respectively. The tables show the effect of the real-world phenomena on each signal separately and combined. Note that the PID controller does not use the velocity and control surface deflections measurements as feedback signals. The tables also show a baseline run without real-world phenomena running at 50 and 100 Hz. Furthermore, the total effect of all real-world phenomena combined is presented. As the constant wind has a significant effect on this number hiding the stability issues of INDI, also the total effect without wind is given.

Table 3: RMS tracking error PID

	Bias	Noise	Delay	Sampling	Baseline (100Hz)
Combined	0.2294	0.1915	0.1749	0.1891	0.1902
p, q, r	0.1902	***0.1902***	***0.1758***	0.189	Baseline (50Hz)
V	n.a.	n.a.	n.a.	n.a.	0.1895
δ_a, δ_e, δ_r	n.a.	n.a.	n.a.	n.a.	Total
ϕ, θ	0.1901	0.1902	0.1921	0.1903	0.4265
n_y	0.2032	0.1902	0.1906	0.1902	Total (-wind)
Wind/Turb.	***0.2428***	0.1913	n.a.	n.a.	***0.1928***

Table 4: RMS tracking error INDI

	Bias	Noise	Delay	Sampling	Baseline (100Hz)
Combined	0.2665	0.1895	0.2083	0.1892	0.1891
p, q, r	0.1891	***0.1891***	***0.2068***	0.1891	Baseline (50Hz)
V	0.1894	0.1891	0.1891	0.1891	0.1888
δ_a, δ_e, δ_r	***0.2129***	0.1891	***0.1914***	0.1891	Total
ϕ, θ	0.1903	0.1891	0.1909	0.1892	0.2604
n_y	0.1897	0.1891	0.1891	0.1891	Total (-wind)
Wind/Turb.	***0.2554***	0.1895	n.a.	n.a.	***0.2396***

Table 5: RMS tracking error INDI+

	Bias	Noise	Delay	Sampling	Baseline (100Hz)
Combined	0.2585	0.1914	0.1825	0.1895	0.191
p, q, r	0.191	***0.191***	***0.1811***	0.1894	Baseline (50Hz)
V	0.1916	0.191	0.191	0.191	0.1909
δ_a, δ_e, δ_r	***0.1929***	0.191	***0.1933***	0.191	Total
ϕ, θ	0.1924	0.191	0.193	0.1911	0.2479
n_y	0.1917	0.191	0.1911	0.191	Total (-wind)
Wind/Turb.	***0.2573***	0.1914	n.a.	n.a.	***0.1846***

Comparing Table 3, Table 4 and output response observations, five simulation runs show significant performance degradation caused by actuator measurement bias, wind bias, angular rate measurement noise, angular rate measurement delay and actuator measurement delay. Sec. V.C discusses solutions to prevent performance degradation due to these phenomena. As seen in Table 5 and Fig. 6f, the performance of INDI significantly improves when these solutions are implemented, referred to as INDI+. Fig. 6 shows the difference in pitch angle response between the INDI and INDI+ controllers for all phenomena causing performance degradation.

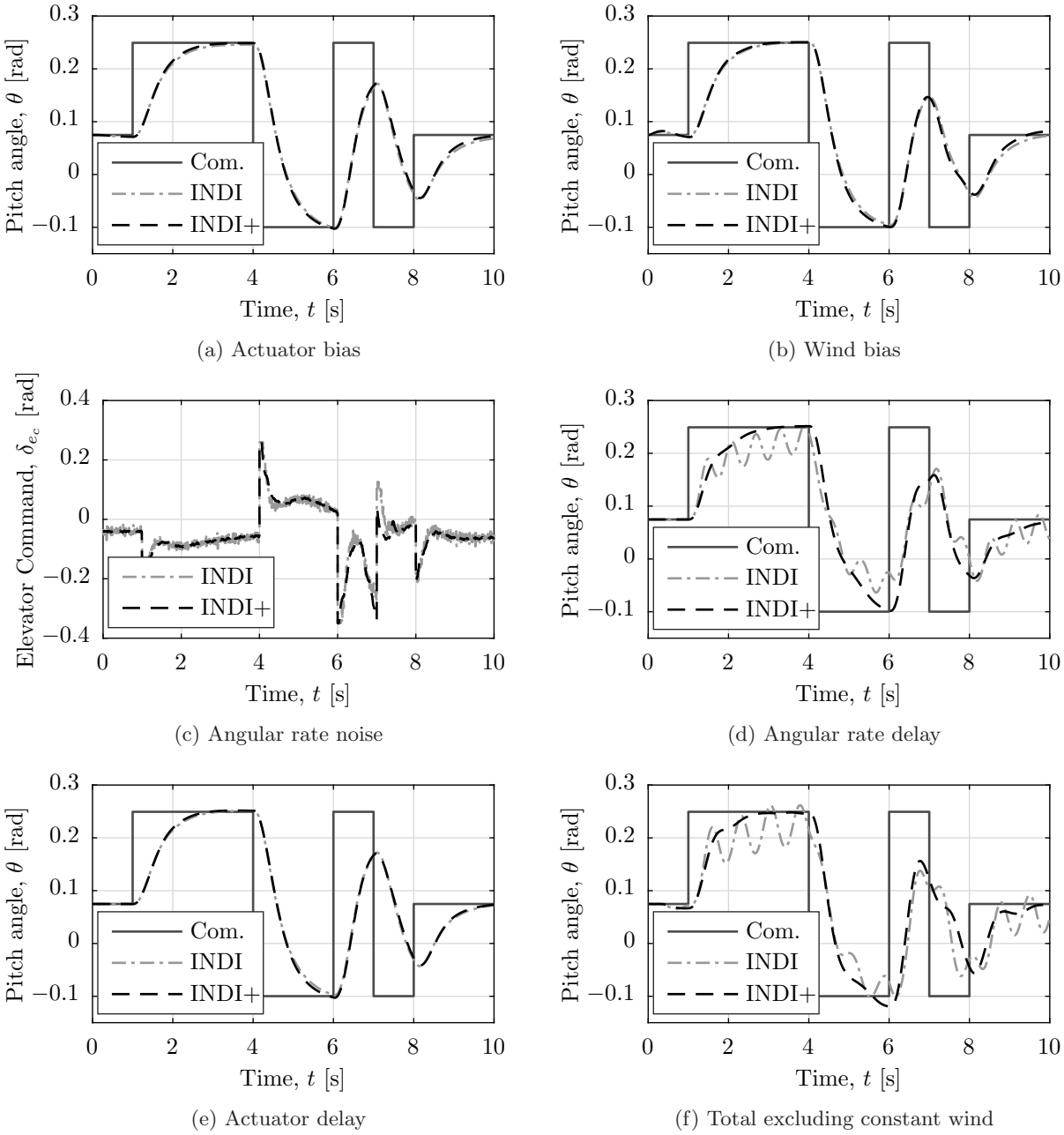

(a) Actuator bias

(b) Wind bias

(c) Angular rate noise

(d) Angular rate delay

(e) Actuator delay

(f) Total excluding constant wind

Figure 6: Pitch response subjected to selected phenomena for INDI with and without solutions

C. Solutions for Performance Degradation

The baseline INDI attitude controller developed in Sec. IV has to be adapted to solve the issues related to real-world phenomena and improve performance. A requirement imposed on the adaptations proposed in this paper is that no additional model dependencies should be added to the controller to avoid losing one of the main benefits of INDI control. First, Fig. 6a shows that a bias on the actuator position measurements causes a steady-state error within the closed-loop response. Initially, a combination of PI-control to design the virtual control input with PCH as anti-windup technique was used to solve the steady-state error. However, when PCH is used based on the latest available actuator measurement, the PCH RM also adapts to the bias in these measurements such that the steady-state error remains.

Two options can be implemented that do eliminate the steady-state error: PCH could be implemented based on an actuator model instead of actuator measurements or the PCH RM could be based on PI-control. The first option has the benefit of having an anti-windup for the integrator element at the expense of additional model dependency within the controller. The second option does not require the actuator model, but also loses the anti-windup benefit. As discussed, the lack of model dependencies, one of the main benefits of INDI control, is considered more important and therefore the second option is selected. Still, Sec. VI shows that PCH is a valuable addition even when the anti-windup benefit is lost.

Second, Fig. 6b shows that the INDI controller has to adapt to the constant wind conditions increasing the RMS tracking error. Fortunately, as expected from literature, the constant wind does not cause a steady-state error as the bias is eventually rejected by the INDI controller.[14] Therefore, no solution is required for this phenomenon.

Third, Fig. 6c shows that differentiation amplifies the noise on the control input signals and signals used for identification in Sec. VI. Implementing a second-order filter, see Eq. (29), on the angular rate measurements can be used to reduce the noise on these signals.[14,26] Using Tustin's transformation, the continuous-time filter of Eq. (29) is converted into the discrete-time equivalent. Adequate filter performance was obtained using $\omega_n = 40$ rad/s and $\zeta = 0.6$.

$$H(s) = \frac{\omega_n^2}{s^2 + 2\zeta\omega_n s + \omega_n^2} \tag{29}$$

Finally, Fig. 6d shows that unsynchronized delays between the actuator and angular rate measurements cause oscillatory behavior. Note that Fig. 6e does not show this behavior as the actuator measurement delay of the PH-LAB is significantly smaller than the angular rate measurement delay, see Table 2. To improve system performance the two signals should be synchronized. This synchronization can partially be performed by filtering the actuator measurements with the exact same filter dynamics as the angular rates, since filters also introduce lag into a system.[14] Moreover, either the actuator or the angular rate measurements can be delayed with a multiple of the controller frequency, such that the delay originating from using different type of sensors and data buses can be eliminated. This does require successful identification of the difference in delay between the two feedback signals, an issue which is discussed in detail in Sec. VI.

VI. Unsynchronized Time Delay

The previous section identified that unsynchronized delays between the actuator and angular rate measurements cause oscillatory behavior. Therefore, successful identification of the difference in delay between the two feedback signals is vital for adequate INDI controller performance. The identified difference can then be added to the appropriate signal to synchronize the time delay.

A. Performance Degradation

First, the performance degradation characteristics due to unsynchronized time delay are investigated. Fig. 7 shows the RMS tracking error as function of both actuator and angular rate delay for an INDI controller with PCH and affected by real-world phenomena. As expected based on the results of Sec. III and Sec. V the best performance is obtained when both delays are about equal. Still, Fig. 7 also shows that a small mismatch between both delays is acceptable. Additionally, with the current controller gains a delay of about 220 ms in both signals results in overall controller degradation. This is 100 ms above the delay of 130 ms identified from PH-LAB flight test data. Furthermore, it can be seen that the controller performance is less sensitive to actuator delay than angular rate delay, as discussed in Sec. III.

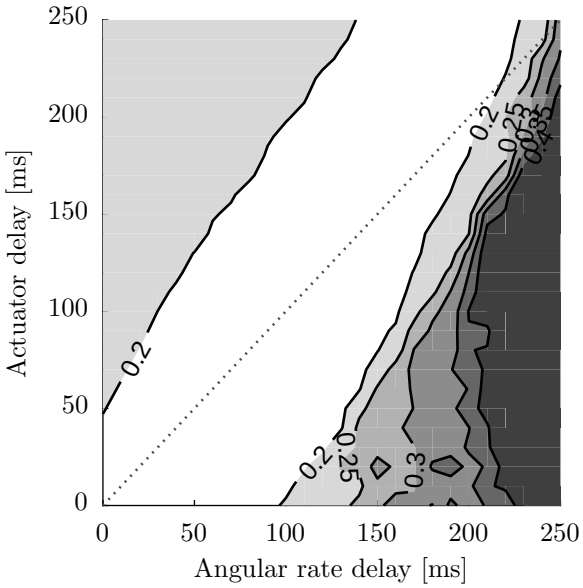

Figure 7: RMS performance for INDI with PCH affected by real-world phenomena

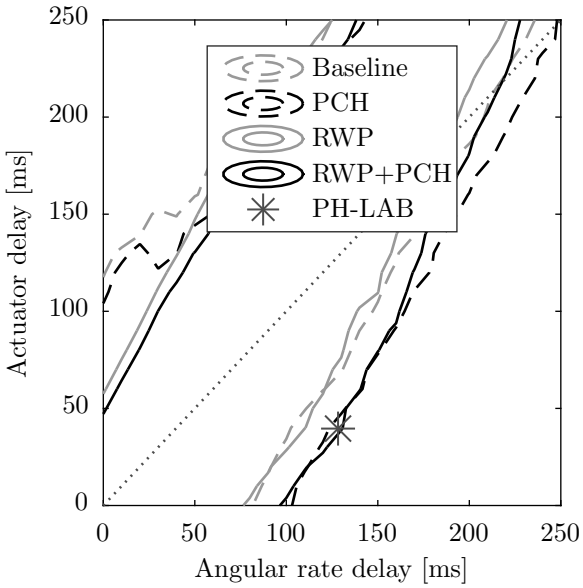

Figure 8: INDI performance boundaries, RMS=0.2, with/without PCH and real-world phenomena

Fig. 8 shows the performance boundaries for the INDI controller with/without real-world phenomena (RWP) and with/without PCH. The performance boundary is set at an RMS of 0.2, which is the value at which oscillatory behavior starts to appear. Fig. 8 shows that the performance of the INDI controlled PH-LAB is degraded independent of which combination of RWP and PCH is taken. The figure also shows that the addition of RWP does slightly reduce the region of adequate performance.

Interestingly, Fig. 8 also shows that the region of adequate performance shifts towards larger angular rate delays when PCH is used. As explained in Sec. IV, the inner loop K_P gain is larger for the controller with PCH compared with the controller without PCH. As such, the influence of the virtual control input, based on the inner loop tracking error, on the actual control input increases compared with the angular rate derivative feedback. This shift in influence reduces performance degradation due to angular rate delay, because the angular rate derivative feedback is the cause of oscillatory behavior leading to performance degradation.

B. Real-Time Time Delay Identification

The real-time time delay identification algorithm used is based on the concept of latency. Latency is the time delay between when a control command is given and the corresponding measurement is collected. The difference in latency between the actuator and angular rate measurements is a measure of the unsynchronized delay between these signals. The latency of the actuator measurement signal is based on control commands of (δ_a, δ_e, δ_r) and the measurements of these signals. The latency of the angular rates is based on the virtual control inputs (ν_p, ν_q, ν_r) and the filtered angular acceleration estimates ($\dot{p}$, $\dot{q}$, $\dot{r}$). Sharp peaks within the signals are most useful for identification, as these are easiest to match between the command and the actual response. Therefore, the derivatives of the mentioned signals are used, as it magnifies those parts of the signals with large derivatives.

To obtain an estimate of the latency of these signals, the average square difference function (ASDF) is used.[27] This function does not introduce additional model dependencies into the controller as only already available signals are used. Moreover, the ASDF is computationally efficient and is not affected by the mean of the signal like, for example, the correlation function. Literature indicates that the ASDF has adequate performance for signals with a signal-to-noise ratio (SNR) larger than 15 dB.[28] Fortunately, the SNR of the flight test signals was estimated around 20 dB, based on the PH-LAB with 3211 maneuvers on pitch and roll angles with a 10 degree magnitude. Other, more complex, algorithms exist in literature that could deal with low SNR signals, when the threshold of 15 dB cannot be met.

The ASDF can be computed by obtaining the argument minimizing Eq. (30).[27] Eq. (30) can be converted into a recursive formula, Eq. (31) to reduce memory and computational resources. Furthermore, the latency of both the roll and pitch channel can be identified separately, after which an average can be used within the controller improving identification accuracy.

$$\hat{R}(\tau) = \frac{1}{N}\sum_{k=1}^{N}[x_1(kT) - x_2(kT+\tau)]^2 \tag{30}$$

$$\hat{R}_k(\tau) = \frac{1}{N_k}[N_{k-1}\hat{R}_{k-1} + (x_{1_{k-\tau}} - x_{2_k})^2] \tag{31}$$

C. Results

The success of the real-time time delay algorithm can be seen in Fig. 9. This figure shows the final delay identification error after the 40 second simulations. The error ranges between -10ms, a surplus in angular delay added to the controller, and 30 ms, a surplus in actuator delay added to the controller. This range shows that it is difficult for the algorithm to perfectly estimate the time delay, however the range is within the region of best performance, based on Fig. 8, up to about 200 ms of total delay. Less aggressive control gains can be used to increase the total delay tolerated. The identification error is mainly caused by the bias, noise and sampling time phenomena. For example, the PH-LAB obtains angular rate measurements with a sampling time of 19.2 ms, while the algorithm tries to identify with a resolution of 10 ms, equivalent to the controller sampling time.

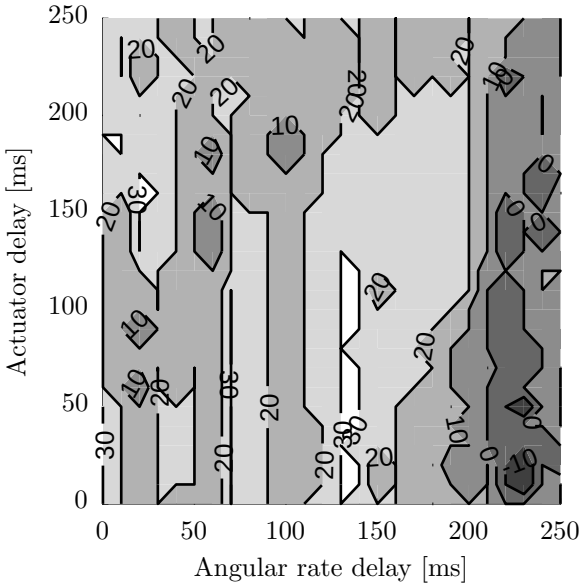

Figure 9: Delay identification error after 40 seconds with real-world phenomena and PCH

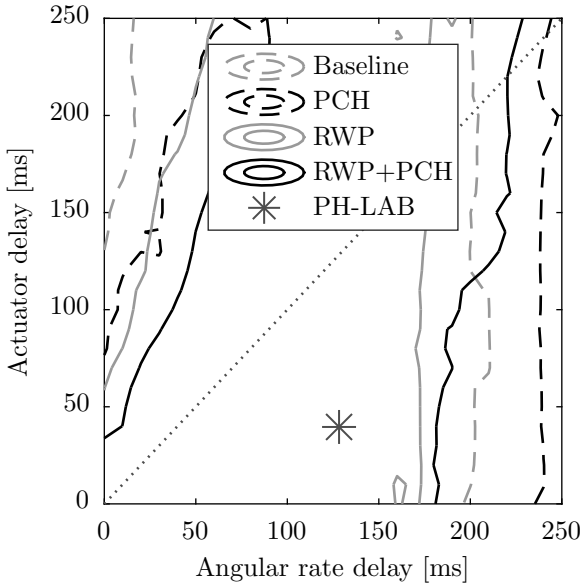

Figure 10: INDI performance boundaries, RMS=0.2, with delay identification

The performance boundaries of INDI with the real-time time delay algorithm activated are given in Fig. 10. Clearly, the performance of INDI has improved compared to Fig. 8, as expected based on the results of Fig. 9. Especially, when it is considered that the left performance boundary is not too important regarding stability, as INDI is not as sensitive to a surplus of actuator delay. Moreover, the performance of the system including PCH and phenomena inevitably degrades for time delays larger than 220 ms, as discussed based on Fig. 7. However, some parts of Fig. 10 still have an RMS larger than 0.2 due to a worse transient response in which the time delay is identified. Besides, Fig. 10 shows that without additional phenomena simulated, the algorithm in combination with PCH has adequate performance up to a total delay of 240 ms.

VII. Conclusion

Incremental nonlinear dynamic inversion (INDI) is a promising control technique that could contribute to safer, cheaper flight control systems (FCSs) with shorter development periods, straightforward certification and increased performance. This paper has shown that performance degradation due to typical aircraft characteristics can be prevented to retain the advantages of INDI as proven on other application platforms.

An analytical stability analysis showed that implementing discrete-time INDI with a smaller sampling time results in larger stability margins regarding system characteristics and controller gains. More specifically, the analysis concluded that sampling times smaller than 0.02s result in large stability margins. Moreover, the artificial unit delay of the actuator measurements implemented by some other authors was found to degrade system stability.

The effect of the real-world phenomena, bias, discretization, noise and time delay on an INDI controlled aircraft were investigated. Four phenomena showed significant performance degradation requiring controller adaptation: actuator measurement bias, angular rate measurement noise, angular rate measurement delay and actuator measurement delay.

Fortunately, the performance degradation can be prevented using a combination of three solutions without introducing additional model dependencies into the controller. First, using PI-control to design the virtual control input of the inner loop prevents a steady-state error due to actuator measurement bias. Second, a second-order low-pass filter can be used to reduce noise in the control input signal due to angular rate measurement noise. Third, the measurement delay of the angular rate and actuator measurements have to be synchronized to prevent oscillatory behavior, although a small mismatch between the delay in both signals is acceptable.

The importance of synchronizing the measurements was confirmed by both the analytical stability analysis and simulations with an INDI controlled aircraft. Moreover, both methods also showed that INDI is inherently more sensitive to a surplus of angular rate delay compared with a surplus of actuator delay. Part of this effect can be counteracted using pseudo control hedging (PCH), which favorably shifts the region of adequate performance towards a surplus of angular rate delay.

To synchronize the measurements a real-time time delay identification algorithm based on the concept of latency was proposed. The latency of both actuator and angular rate measurements with respect to the values commanded by the controller are identified using the average square difference function (ASDF). The difference in latency between the actuator and angular rate measurements is a measure of the unsynchronized delay between these signals. The unsynchronized delay is successfully identified by the algorithm with only a small error range. As such, the controller can fly with each combination of actuator and angular rate delay for values well above typical delays for aircraft. An additional benefit of the algorithm is that it does not introduce additional model dependencies into the controller as only already available signals are used.

References

[1]Balas, G. J., "Flight Control Law Design: An Industry Perspective," *European Journal of Control*, Vol. 9, No. 2-3, 2003, pp. 207–226.

[2]Balas, G. J. and Hodgkinson, J., "Control Design Methods for Good Flying Qualities," *AIAA Atmospheric Flight Mechanics Conference*, AIAA, Chicago, IL, USA, 2009.

[3]Enns, D., Bugajski, D., Hendrick, R., and Stein, G., "Dynamic Inversion: An Evolving Methodology for Flight Control Design," *International Journal of Control*, Vol. 59, No. 1, 1994, pp. 71–91.

[4]Walker, G. P. and Allen, D. A., "X-35B STOVL Flight Control Law Design and Flying Qualities," *2002 Biennial International Powered Lift Conference and Exhibit*, AIAA, Williamsburg, VA, USA, 2002.

[5]Lombaerts, T. J. J., Huisman, H. O., Chu, Q. P., Mulder, J. A., and Joosten, D. A., "Nonlinear Reconfiguring Flight Control based on Online Physical Model Identification," *Journal of Guidance, Control, and Dynamics*, Vol. 32, No. 3, 2009, pp. 727–748.

[6]Anon., "Civil Aviation Safety Data: 1993-2007," Tech. rep., Civil Aviation Authority of the Netherlands (CAANL), The Hague, the Netherlands, 2008.

[7]Anon., "State of Global Aviation Safety," Tech. rep., International Civil Aviation Organization (ICAO), Montreal, Canada, 2013.

[8]Sieberling, S., Chu, Q. P., and Mulder, J. A., "Robust Flight Control using Incremental Nonlinear Dynamic Inversion and Angular Acceleration Prediction," *Journal of Guidance, Control, and Dynamics*, Vol. 33, No. 6, 2010, pp. 1732–1742.

[9]Johnson, E. N. and Kannan, S. K., "Adaptive Trajectory Control for Autonomous Helicopters," *Journal of Guidance, Control, and Dynamics*, Vol. 28, No. 3, 2005, pp. 524 – 538.

[10]Heise, C. D., Falconí, G. P., and Holzapfel, F., "Hexacopter Outdoor Flight Test Results of an Extended State Observer

based Controller," *2014 IEEE International Conference on Aerospace Electronics and Remote Sensing Technology*, IEEE, Yogyakarta, Indonesia, 2014, pp. 26–33.

[11]Acquatella B., P., Falkena, W., van Kampen, E.-J., and Chu, Q. P., "Robust Nonlinear Spacecraft Attitude Control using Incremental Nonlinear Dynamic Inversion," *AIAA Guidance, Navigation, and Control Conference*, AIAA, Minneapolis, MN, USA, 2012.

[12]Simplício, P., Pavel, M. D., van Kampen, E., and Chu, Q. P., "An Acceleration Measurements-based Approach for Helicopter Nonlinear Flight Control using Incremental Nonlinear Dynamic Inversion," *Control Engineering Practice*, Vol. 21, No. 8, 2013, pp. 1065–1077.

[13]Smith, P. and Berry, A., "Flight Test Experience of a Non-Linear Dynamic Inversion Control Law on the VAAC Harrier," *Atmospheric Flight Mechanics Conference*, AIAA, Denver, CO, USA, 2000, pp. 132–142.

[14]Smeur, E. J. J., Chu, Q. P., and de Croon, G. C. H. E., "Adaptive Incremental Nonlinear Dynamic Inversion for Attitude Control of Micro Air Vehicles," *Journal of Guidance, Control, and Dynamics*, Vol. 39, No. 3, 2016, pp. 450–461.

[15]Mulder, J. A., van der Vaart, J. C., and Mulder, M., *AE4304: Atmospheric Flight Dynamics*, Faculty of Aerospace Engineering, Delft University of Technology, Delft, the Netherlands, 2007.

[16]Nise, N. S., *Control Systems Engineering*, John Wiley & Sons, Inc., Asia, 6th ed., 2011.

[17]Jury, E. I., "A Modified Stability Table for Linear Discrete Systems," *Proceedings of the IEEE*, Vol. 53, No. 2, 1965, pp. 184–185.

[18]Lu, P. and van Kampen, E.-J., "Active Fault-Tolerant Control for Quadrotors Subjected to a Complete Rotor Failure," *2015 IEEE/RSJ International Conference on Intelligent Robots and Systems*, IEEE/RSJ, Hamburg, Germany, 2015, pp. 4698–4703.

[19]Miller, C. J., "Nonlinear Dynamic Inversion Baseline Control Law: Architecture and Performance Predictions," *AIAA Guidance, Navigation, and Control Conference*, AIAA, Portland, OR, USA, 2011.

[20]Lombaerts, T. J. J. and Looye, G. H. N., "Design and Flight Testing of Nonlinear Autoflight Control Laws," *AIAA Guidance, Navigation, and Control Conference*, AIAA, Minneapolis, MN, USA, 2012.

[21]Lombaerts, T. J. J. and Looye, G. H. N., "Design and Flight Testing of Manual Nonlinear Flight Control Laws," *AIAA Guidance, Navigation, and Control Conference*, AIAA, Portland, OR, USA, 2011.

[22]Johnson, E. N. and Calise, A. J., "Pseudo-Control Hedging: A New Method for Adaptive Control," *Advances in Navigation Guidance and Control Technology Workshop*, Redstone Arsenal, AL, USA, 2000.

[23]Schierman, J. D., Ward, D. G., Hull, J. R., Gandhi, N., Oppenheimer, M. W., and Doman, D. B., "Integrated Adaptive Guidance and Control for Re-Entry Vehicles with Flight-Test Results," *Journal of Guidance, Control, and Dynamics*, Vol. 27, No. 6, 2004, pp. 975–988.

[24]Johnson, E. N. and Turbe, M. A., "Modeling, Control, and Flight Testing of a Small Ducted-Fan Aircraft," *Journal of Guidance, Control, and Dynamics*, Vol. 29, No. 4, 2006, pp. 769 – 779.

[25]Bauschat, J.-M., Mönnich, W., Willemsen, D., and Looye, G., "Flight Testing Robust Autoland Control Laws," *AIAA Guidance, Navigation, and Control Conference and Exhibit*, AIAA, Montreal, Canada, 2001.

[26]Bacon, B. J., Ostroff, A. J., and Joshi, S. M., "Reconfigurable NDI Controller using Inertial Sensor Failure Detection & Isolation," *IEEE Transactions on Aerospace and Electronic Systems*, Vol. 37, No. 4, 2001, pp. 1373–1383.

[27]Jacovitti, G. and Scarano, G., "Discrete Time Techniques for Time Delay Estimation," *IEEE Transactions on Signal Processing*, Vol. 41, No. 2, 1993, pp. 525–533.

[28]Nandi, A. K., "On the Subsample Time Delay Estimation of Narrowband Ultrasonic Echoes," *IEEE Transactions on Ultrasonics Ferroelectrics and Frequency Control*, Vol. 42, No. 6, 1995, pp. 993–1002.